



## Effect of volcanic aerosol on stratospheric NO<sub>2</sub> and N<sub>2</sub>O<sub>5</sub> from 2002-2014 as measured by Odin-OSIRIS and Envisat-MIPAS

5 Cristen Adams<sup>1,2</sup>, Adam E. Bourassa<sup>1</sup>, Chris A. McLinden<sup>3</sup>, Chris E. Sioris<sup>3</sup>, Thomas von Clarmann<sup>4</sup>,  
Bernd Funke<sup>5</sup>, Landon A. Rieger<sup>1</sup>, and Douglas A. Degenstein<sup>1</sup>

<sup>1</sup>Institute of Space and Atmospheric Studies, University of Saskatchewan, Saskatoon, Canada.

<sup>2</sup>Alberta Environmental Monitoring, Evaluation, and Reporting Agency, Edmonton, Alberta, Canada

<sup>3</sup>Environment and Climate Change Canada, Downsview, Ontario, Canada.

<sup>4</sup>Karlsruhe Institute of Technology, Institute for Meteorology and Climate Research, Karlsruhe, Germany.

10 <sup>5</sup>Instituto de Astrofísica de Andalucía, CSIC, Granada, Spain

Correspondence to: Cristen Adams (cristenfadams@gmail.com)

**Abstract.** Following the large volcanic eruptions of Pinatubo in 1991 and El Chichón in 1982, decreases in stratospheric NO<sub>2</sub> associated with enhanced aerosol were observed. The Optical Spectrograph and InfraRed Imaging Spectrometer (OSIRIS) likewise measured widespread enhancements of stratospheric aerosol following seven volcanic eruptions between 2002 and 2014, although the magnitudes of these eruptions were all much smaller than the Pinatubo and El Chichón eruptions. In order to isolate and quantify the relationship between volcanic aerosol and NO<sub>2</sub>, NO<sub>2</sub> anomalies were calculated using measurements from OSIRIS and the Michelson Interferometer for Passive Atmospheric Sounding (MIPAS). In the tropics, variability due to the quasi-biennial oscillation was subtracted from the timeseries. OSIRIS profile measurements indicate that the strongest relationships between NO<sub>2</sub> and volcanic aerosol extinction were for the layer ~3-7 km above the tropopause, where OSIRIS stratospheric NO<sub>2</sub> partial columns for ~3-7 km above the tropopause were found to be smaller than baseline levels during these aerosol enhancements by up to ~60% with typical Pearson correlation coefficients of  $R \sim -0.7$ . MIPAS also observed decreases in NO<sub>2</sub> partial columns during periods of affected by volcanic aerosol, with percent differences of up to ~25%. An even stronger relationship was observed between OSIRIS aerosol optical depth and MIPAS N<sub>2</sub>O<sub>5</sub> partial columns, with  $R \sim -0.9$ , although no link with MIPAS HNO<sub>3</sub> was observed. The variation of OSIRIS NO<sub>2</sub> with increasing aerosol was found to be quantitatively consistent with simulations from a photochemical box model in terms of both magnitude and degree of non-linearity.

15  
20  
25



## 1 Introduction

Major volcanic eruptions can increase levels of sulfate aerosols in the stratosphere, which provide surfaces on which heterogeneous chemical reactions take place. This, in turn, can affect photochemistry with some of the largest impacts expected for the partitioning of reactive nitrogen,  $\text{NO}_y$  (where  $\text{NO}_y = \text{NO} + \text{NO}_2 + \text{HNO}_3 + \text{N}_2\text{O}_5 + \text{ClONO}_2 + \text{BrONO}_2$ ) species (e.g., Coffey, 1996). The two key heterogeneous reactions that compete with gas-phase chemistry at all stratospheric temperatures are (1) and (2), below (e.g., Cohen and Murphy, 2003). In the presence of volcanic aerosol, the rate of  $\text{N}_2\text{O}_5$  conversion to  $\text{HNO}_3$  increases as shown in Eq. (1):



leading to an increase in levels of  $\text{HNO}_3$ , and a decrease in levels of  $\text{N}_2\text{O}_5$ . Since  $\text{N}_2\text{O}_5$  is a reservoir species for  $\text{NO}_x$ , levels of  $\text{NO}_x$  also decrease. The hydrolysis of  $\text{BrONO}_2$ , shown in Eq. (2):



can also lead to decreased levels of  $\text{NO}_2$  in the lower stratosphere, which are particularly significant toward high latitudes in the summer (Randeniya et al., 1997). The hydrolysis of chlorine nitrate can also play a significant role inside the polar vortex, (Wegner et al., 2012), but is not considered here because measurements were taken outside the polar vortex.

Following the large 1982 and 1991 El Chichón and Pinatubo volcanic eruptions, several studies measured significant decreases in  $\text{NO}_2$ . Total columns of  $\text{NO}_2$  measured by ground-based instruments decreased by ~15-70% following these eruptions (Coffey, 1996; Johnston et al., 1992; Koike et al., 1993; Mills et al., 1993). Fahey et al. (1993) measured in situ  $\text{NO}_x/\text{NO}_y$  aboard aircraft following Pinatubo and found that  $\text{NO}_x/\text{NO}_y$  decreased with aerosol surface area, with a saturation effect toward larger aerosol surface areas.

The effect of the Pinatubo eruption on  $\text{HNO}_3$  and  $\text{N}_2\text{O}_5$  were also assessed in several studies. Some studies noted increases in  $\text{HNO}_3$  and attributed these increases to Eq. (1), but this was not consistently observed across various ground-based, in situ, and satellite datasets (e.g., Coffey, 1996; Rinsland et al., 1994). Rinsland et al. (1994) found decreases in  $\text{N}_2\text{O}_5$  following Pinatubo, which is also consistent with Eq. (1).

The Optical Spectrograph and InfraRed Imaging System (OSIRIS) has observed enhancements in stratospheric aerosol from multiple volcanoes since it began taking measurements in 2001 (Bourassa et al., 2012a). The effect of these more recent volcanoes on stratospheric  $\text{NO}_2$ , also measured by OSIRIS, is investigated in the present study. Stratospheric  $\text{SO}_2$ ,  $\text{NO}_2$ ,  $\text{HNO}_3$ , and  $\text{N}_2\text{O}_5$  from the Michelson Interferometer for Passive Atmospheric Sounding (MIPAS) are also considered. Variations in



NO<sub>2</sub>, HNO<sub>3</sub> and N<sub>2</sub>O<sub>5</sub> with aerosol are also studied using a photochemical box model. To the authors' knowledge, this is the first study that measures the effect of increased volcanic aerosol on NO<sub>2</sub>, HNO<sub>3</sub>, or N<sub>2</sub>O<sub>5</sub> following these smaller more-recent eruptions.

This paper is organized as follows. The OSIRIS, MIPAS, and photochemical model datasets are described in Sect. 2. Monthly average NO<sub>2</sub>, HNO<sub>3</sub>, and N<sub>2</sub>O<sub>5</sub> anomalies and baseline values are calculated from these data using the methodology given in Sect. 3. The relationships between these anomalies and volcanic aerosol measured by OSIRIS are presented in Sect. 4, with conclusions given in Sect. 5.

## 2. Satellite and model datasets

### 2.1 OSIRIS MART aerosol extinction and NO<sub>2</sub>

OSIRIS (Llewellyn et al., 2004; McLinden et al., 2012) is a Canadian satellite instrument on-board the Odin spacecraft (Murtagh et al., 2002), which was launched 20 February 2001 into a sun-synchronous orbit at ~600 km altitude and a descending node equatorial crossing time of ~06:30 local time (LT). OSIRIS measures limb-scattered radiances with near-global coverage in the summer hemisphere from 82°S to 82°N.

The OSIRIS Multiplicative Algebraic Reconstruction Technique (MART) v5.07 NO<sub>2</sub> (Bourassa et al., 2011) and aerosol extinction at 750 nm (Bourassa et al., 2007) data products were used for this study. Data were collected by the optical spectrograph, which measures from 280-810 nm, with a ~1 nm spectral resolution using an optical grating and a charge-coupled device detector. The SASKTRAN spherical forward model is used in the inversion and accounts for multiple scattering and ground albedo (Bourassa et al., 2008). OSIRIS MART aerosol extinction is consistent with SAGE III to ~10% (Bourassa et al., 2012b) and to within ~20% with SAGE II, although the conversion to 525 nm makes the comparison more difficult (Rieger et al., 2015). The OSIRIS MART NO<sub>2</sub> data product is consistent with the OSIRIS Chalmers NO<sub>2</sub> data product (Bourassa et al., 2011).

For both aerosol extinction and NO<sub>2</sub>, OSIRIS data from the descending node, with solar zenith angle (SZA) < 88° were used in this analysis. For aerosol, an extinction threshold of > 2x10<sup>-3</sup> km<sup>-1</sup> was used to terminate the profiles at lower altitudes. This excludes some lower stratospheric altitudes where an aerosol saturation effect occurs in fresh volcanic plumes (Fromm et al., 2014). Similarly, values of NO<sub>2</sub> > 5x10<sup>9</sup> mol/cm<sup>3</sup> were removed from the profiles. Data below the thermal tropopause, calculated using lapse rates from the National Center for Environmental Prediction (NCEP) reanalysis data (Kalnay et al., 1996), were excluded. As discussed further in Sect. 2.3, below, in order to account for the diurnal variation of NO<sub>2</sub>, a photochemical model (Brohede et al., 2008; McLinden et al., 2000) was used to scale all NO<sub>2</sub> profiles to a common local time



of 06:30 LT. Profiles for SZA at 06:30 LT > 88° were also excluded from the analysis in order to prevent scaling data to periods near sunrise when NO<sub>2</sub> is varying rapidly.

## 2.2 MIPAS IMK/IAA SO<sub>2</sub>, NO<sub>2</sub>, N<sub>2</sub>O<sub>5</sub>, and HNO<sub>3</sub>

MIPAS (Fischer et al., 2008) is on board the Environmental Satellite (Envisat), which was launched on 1 March 2002 into a Sun-synchronous polar orbit at 800 km altitude with 14.4 orbits per day. MIPAS measured limb radiances in the mid-infrared from 4.1-14.7 μm (685-2410 cm<sup>-1</sup>) until communication with the satellite was lost in April 2012.

For this study, SO<sub>2</sub>, N<sub>2</sub>O<sub>5</sub>, HNO<sub>3</sub>, and NO<sub>2</sub> from retrievals performed by the Institute of Meteorology and Climate Research (IMK) and Instituto de Astrofísica de Andalucía (IAA) were used. The version V5R\_NO2\_220/V5R\_NO2\_221, V5R\_N2O5\_220/V5R\_N2O5\_221, V5R\_HNO3\_224/V5R\_HNO3\_225, V5R\_SO2\_220/V5R\_SO2\_221 data from January 2005 to April 2012 were considered. Prior to 2005, data are available, but MIPAS operated with a different spectral resolution and only minor volcanic eruptions occurred. Retrievals for NO<sub>2</sub> (Funke et al., 2005, 2014), N<sub>2</sub>O<sub>5</sub> (Mengistu Tsidu et al., 2004), HNO<sub>3</sub> (von Clarmann et al., 2009), and SO<sub>2</sub> (Höpfner et al., 2013) are performed using a constrained multiparameter nonlinear least squares fitting of measured and modelled spectra (von Clarmann et al., 2009). Data unaffected by clouds and with diagonal terms of the averaging kernel > 0.03 were used for the analysis. Only daytime measurements (SZA < 88°), taken at 10 LT, were used for consistency with OSIRIS.

## 2.3 Photochemical modelling

A stratospheric photochemical box model (Brohede et al., 2008; McLinden et al., 2000) was used to help interpret the satellite data. The model is constrained with climatological profiles of ozone and temperature. Long-lived species (N<sub>2</sub>O, CH<sub>4</sub>, H<sub>2</sub>O) and families (NO<sub>y</sub>, Cl<sub>y</sub>, Br<sub>y</sub>) are based on a combination of three-dimensional model output or trace-correlations. All remaining species are calculated to be in a 24-hour steady-state by integrating the model over 30 days, but fixed to a specified Julian day. Heterogeneous chemistry on background stratospheric aerosols is included using the aerosol surface area climatology of Thomason et al. (1997), but polar stratospheric clouds are not included. Brohede et al. (2008) demonstrated that this model can accurately simulate stratospheric nitrogen partitioning.

The model is typically used for two purposes: (i) to adjust the local time of the OSIRIS measurements to a common value through a photochemical scaling factor (e.g., Brohede et al., 2008, 2007), and (ii) to model the behavior of NO<sub>2</sub> and other species for varying levels of aerosol. In this latter application, the aerosol surface area, SA (μm<sup>2</sup>/cm<sup>3</sup>), is adjusted so that it matches the extinction coefficient, *k* (km<sup>-1</sup>), measured by the OSIRIS instrument, which are related through the expression,

$$SA(z) = \frac{4000}{\bar{q}} \cdot k(z) \quad , \quad (3)$$



and where the conversion involves the effective scattering efficiency,  $\bar{Q}$  (e.g., Hansen and Travis, 1974). The scattering efficiency was calculated using Mie theory to be 0.40 for background spherical sulfate particles (with mode radius of 0.08  $\mu\text{m}$ ). Following an eruption, the efficiency will be modified as the size distribution changes.  $\text{SO}_2$  will rapidly form sulfuric acid, which can condense to form new small particles or increase the size of existing ones. The Kasatochi eruption, considered here, led to a decrease in stratospheric particle size (Sioris et al., 2010) whereas Sarychev, also considered here, saw an increase in size (O'Neill et al., 2012). As a result of these mixed findings, we elected to keep the scattering efficient constant, using  $SA = 10000 \cdot k$ , but tested a non-linear  $SA$  dependence on  $k$ , analogous to that from Thomason et al. (1997), and incorporated it into an uncertainty. For this, we considered  $SA \propto k^p$  with  $p=1.3$  for an increase in particle size following an eruption, and  $p=0.7$  for a decrease. Furthermore, to account for potential errors in our background  $SA$ , we scaled 10000 by factors of 3 and 1/3 and folded these into the overall uncertainty.

### 3 Calculation of monthly averages, anomalies, and baseline levels

#### 3.1 OSIRIS and MIPAS

Volcanic eruptions and periods affected by volcanic aerosol were identified using monthly averages of latitude-binned OSIRIS aerosol extinction. In order to isolate the effect of volcanic aerosol on  $\text{NO}_2$ ,  $\text{HNO}_3$ , and  $\text{N}_2\text{O}_5$ , anomalies and baseline levels in the absence of volcanic aerosol were estimated for each month and latitude. Partial vertical column densities (VCDs) and partial aerosol optical depth (AOD), as well as vertical profiles were considered. Calculations were made for each month and latitude, and for the profiles, each altitude layer was considered separately. The steps for these calculations are described in the paragraphs below.

Monthly average profiles of aerosol extinction,  $\text{SO}_2$ ,  $\text{NO}_2$ ,  $\text{N}_2\text{O}_5$ , and  $\text{HNO}_3$  were calculated in  $10^\circ$  latitude bins. At least five measurements were required for each bin. Partial column AOD and partial VCDs of  $\text{SO}_2$ ,  $\text{NO}_2$ ,  $\text{N}_2\text{O}_5$ , and  $\text{HNO}_3$  were all calculated from the sum of these monthly mean profiles for the five measurement layers from 3-7 km above the mean NCEP thermal tropopause at each latitude. This altitude range typically corresponded to the highest levels of volcanic aerosol observed by OSIRIS. MIPAS volume mixing ratio profiles were converted to number densities using MIPAS temperature and pressure profiles. Note the calculated VCDs for OSIRIS and MIPAS are offset by 0.5 km because their measurement altitude grids are offset by 0.5 km. MIPAS degrees of freedom for signal (DOFS) were calculated from the trace of the averaging kernel over the partial column altitude range. MIPAS VCDs with DOFS  $< 0.5$  were excluded from the analysis, leaving mean DOFS of 1.3 for  $\text{SO}_2$ , 0.7 for  $\text{NO}_2$ , 1.8 for  $\text{N}_2\text{O}_5$ , and 2.1 for  $\text{HNO}_3$ .

Bins affected by volcanic aerosol were identified using thresholds based on OSIRIS aerosol extinction measurements. For the partial AODs, this threshold was set at  $2 \times 10^{-3}$ , which was approximately the 75<sup>th</sup> percentile of monthly mean partial column



AODs across all latitudes for 50°S to 80°N. For the profiles, the threshold was set using an extinction ratio = 1.2, which was approximately the 90-95<sup>th</sup> percentile of monthly mean extinction ratios across all latitudes for 50°S to 80°N. The extinction ratio (OSIRIS-measured extinction divided by the Rayleigh extinction) has less dependence on altitude than the extinction and was calculated using air density profiles from European Centre for Medium-Range Weather Forecasts analysis data.

- 5 In order to remove the seasonal variation from the NO<sub>2</sub> timeseries, for each bin of the monthly mean NO<sub>2</sub> profiles and VCDs, the NO<sub>2</sub> anomaly ( $dNO_2$ ) was calculated:

$$dNO_2(y, m, lat) = NO_2(y, m, lat) - \overline{NO_2^{NoVolc}(m, lat)} \quad , \quad (4)$$

where  $NO_2(y, m, lat)$  is the NO<sub>2</sub> for the given year/month/latitude bin, and  $\overline{NO_2^{NoVolc}(m, lat)}$  is the mean of binned NO<sub>2</sub> values for the given month across all years for bins that were not affected by volcanic aerosol, as determined by the extinction  
10 thresholds. For the profile analysis, the NO<sub>2</sub> anomaly was calculated separately at each altitude.

The quasi-biennial oscillation (QBO), with a mean period of ~28 months, is the dominant internal mode of climatic variability in the tropical stratosphere (see review by Baldwin et al., 2001). NO<sub>2</sub> can vary by > 25% in the tropics near the tropopause due to QBO (Hauchecorne et al., 2010), which is on the same order of magnitude of the variation of NO<sub>2</sub> observed during periods of enhanced volcanic aerosol in this study. Therefore, the QBO was fit using a robust regression to the NO<sub>2</sub> anomaly  
15 timeseries for each latitude bin between 40°S to 40°N. Bins that were affected by volcanic aerosol were excluded from the fit. The fit was only performed if at least ten NO<sub>2</sub> anomaly values were available, and included the first two principal components of QBO, calculated with stratospheric winds from <http://www.geo.fu-berlin.de/en/met/ag/strat/produkte/qbo/index.html> (Naujokat, 1986). The two QBO principal components and 40°S to 40°N latitude range were selected based on the results of Bourassa et al. (2014). The QBO fits were subtracted from the NO<sub>2</sub> anomaly timeseries for each latitude bin between 40°S to  
20 40°N. For the profile analysis, this procedure was applied separately at each altitude.

An example of the QBO fitting procedure is shown for 20.5 km at 0° latitude in Figure 1. The timeseries of extinction ratios shows several distinct periods with extinction ratios above the extinction ratio threshold of 1.2 (panel a). The QBO fit to the NO<sub>2</sub> anomaly timeseries includes only data collected during time-periods with extinction ratio < 1.2 (panel b) in order to avoid fitting out some of the variability due to volcanic aerosol. The fit includes a constant and the two QBO principal component  
25 terms only. After subtracting the fit, the NO<sub>2</sub> anomaly timeseries has stronger negative anomalies during the periods with enhanced volcanic eruptions (panel c).

Baseline NO<sub>2</sub> profiles and VCDs were also estimated for periods that are not affected by volcanic aerosol. For mid-latitudes and high latitudes (50°S – 80°S and 50°N – 80°N),  $\overline{NO_2^{NoVolc}(m, lat)}$  was used directly for baseline NO<sub>2</sub>. For 40°S – 40°S,



the  $\text{NO}_2$  response to the QBO was added to  $\overline{\text{NO}_2^{\text{No Volc}}(m, lat)}$  in order to estimate the variation of baseline  $\text{NO}_2$  with the QBO. The addition of the QBO signal had a minor impact on this analysis (~5-10%).

The percent difference in  $\text{NO}_2$  ( $100\% \times \frac{\text{NO}_2 \text{ Anomaly}}{\text{Baseline NO}_2}$ ) was used for all figures and calculation of correlation coefficients in this study. Replacing percent difference  $\text{NO}_2$  with the  $\text{NO}_2$  anomaly has a minor influence on the shape of scatter plots and Pearson correlation coefficients (R) between  $\text{NO}_2$  and aerosol extinction.

For  $\text{N}_2\text{O}_5$  and  $\text{HNO}_3$ , anomalies and baseline values were calculated using the same approach as for  $\text{NO}_2$ . For aerosol extinction profiles and partial AODs, variations due to seasonal cycles are small and variations due to QBO in the tropics are < 10% for 20-26 km (Hommel et al., 2015), while volcanic perturbations in aerosol extinction are often > 100%. Therefore, monthly averages of aerosol extinction and partial AODs were used directly in this analysis, without calculation of anomalies or baseline values.

### 3.2 Photochemical model

A similar approach was used to assess variations in modelled aerosol extinction,  $\text{NO}_2$ ,  $\text{N}_2\text{O}_5$ , and  $\text{HNO}_3$  partial VCDs and profiles. The photochemical model was run monthly at  $10^\circ$  latitude intervals for a range of aerosol surface areas at the approximate OSIRIS measurement time (06:30 LT). For the column amounts, partial VCDs and partial column AODs were calculated over the layers ~3-7 km above the tropopause for each of the model runs. Then, for each latitude and month, percent differences in  $\text{NO}_2$ ,  $\text{N}_2\text{O}_5$ , and  $\text{HNO}_3$  partial VCDs were calculated for a range of partial column AODs using ( $100\% \times \frac{\text{NO}_2(\text{AOD}) - \text{Baseline NO}_2}{\text{Baseline NO}_2}$ ), where  $\text{NO}_2(\text{AOD})$  is the modelled  $\text{NO}_2$  for the given AOD/month/latitude and  $\text{Baseline NO}_2$  is the modelled  $\text{NO}_2$  for the given month/latitude, interpolated to the baseline partial column AOD. The baseline partial column AOD was calculated from OSIRIS measurements at the given latitude. For the profiles, a similar interpolation procedure was used at each altitude layer using OSIRIS-measured aerosol extinction.

### 3.3 Conversions between partial column AODs, aerosol extinction, and extinction at various wavelengths

All AODs and aerosol extinctions presented here are for 750 nm, which is the wavelength of the OSIRIS retrievals. The partial column AODs are for a 5 km altitude range, and therefore can be related to the mean extinction ( $\text{km}^{-1}$ ) over the given altitude range by dividing the partial column AOD by 5. In order to convert aerosol extinctions from 750 nm to other typical wavelengths, the conversion factors given in Table 1 can be used.



## 4 Results

### 4.1 NO<sub>2</sub>, N<sub>2</sub>O<sub>5</sub>, and HNO<sub>3</sub> VCDs

We first examine an example of the modelled variation of NO<sub>2</sub>, N<sub>2</sub>O<sub>5</sub>, and HNO<sub>3</sub> partial VCDs with volcanic aerosol, shown in Figure 2 for 60°N in August. This latitude was affected by enhanced volcanic aerosol in August from the 2009 Sarychev Peak and the 2011 Nabro eruptions, as discussed in further detail below. The maximum partial column AOD observed by OSIRIS at this latitude,  $8 \times 10^{-3}$ , is indicated on the figure. Levels of NO<sub>2</sub> decrease almost exponentially toward larger partial column AODs, reaching percent differences of -45% relative to baseline levels for AOD= $8 \times 10^{-3}$  at the approximate local time of OSIRIS measurements. At the MIPAS local time, reductions in NO<sub>2</sub> are slightly smaller, reaching -40% for AOD= $8 \times 10^{-3}$ . Percent differences in N<sub>2</sub>O<sub>5</sub> decrease even more steeply than NO<sub>2</sub>, reaching up to -86% relative to baseline levels for AOD= $8 \times 10^{-3}$ . HNO<sub>3</sub> increases slightly with partial column AOD, but is only +5% higher than baseline levels for AOD= $8 \times 10^{-3}$ . This is because HNO<sub>3</sub> is the dominant NO<sub>y</sub> species in the lower stratosphere. Therefore, even major changes in the partitioning due to heterogeneous chemistry on sulfate aerosol would have only a marginal relative impact on HNO<sub>3</sub>.

Turning to the measurements, seven periods with volcanic aerosol enhancements were identified in the OSIRIS AOD timeseries, most of which were associated with negative NO<sub>2</sub> anomalies. This is apparent in the timeseries of AOD and percent difference NO<sub>2</sub> VCDs, shown in Figure 3 and summarized in Table 2. Note that only volcanoes with clear signals in the OSIRIS AODs are identified here, and therefore this is not a comprehensive list of all volcanoes known to have influenced the stratosphere.

For some of these volcanic eruptions, a brief signature in MIPAS SO<sub>2</sub> partial VCDs is also apparent during the early part of the AOD enhancements. Stronger SO<sub>2</sub> enhancements are observed after the higher latitude 2008 Mt Okmok / Kasatochi and 2009 Sarychev Peak eruptions. Weaker enhancements are observed after the tropical 2006 Soufrière Hills and 2011 Nabro eruptions. The weaker signal in the tropics is likely because the conversion to sulfate is faster in the tropics due to higher levels of OH. Furthermore, in the tropics, the relative humidity in the troposphere is higher, increasing the scavenging by frozen hydrometeors that trap SO<sub>2</sub> as the eruption column rises through the troposphere (Rodríguez et al., 2008; Textor, 1999). No obvious enhancement in SO<sub>2</sub> was observed after the 2010 Mt Merapi volcano, which is consistent with the weaker signal in OSIRIS AOD for this volcano. MIPAS SO<sub>2</sub> data did not meet the filtering criteria for this study following the 2005 Mt Manam eruption and was unavailable for the 2014 Kelut eruption.

The OSIRIS NO<sub>2</sub> percent differences compared to baseline levels are largely negative during the AOD enhancements (cyan contours) and return to baseline levels when AODs decrease. This is consistent with reduction in NO<sub>2</sub> due to heterogeneous chemistry on the surface of sulfate aerosol. In the MIPAS data, NO<sub>2</sub> anomalies tend to be negative during periods affected by volcanic aerosol. However, this relationship is weaker than observed with the OSIRIS NO<sub>2</sub> data and MIPAS measurements



are not available for the largest observed OSIRIS AODs, as they did not meet the filtering criteria for this study. The variability of  $\text{NO}_2$  outside periods of volcanic aerosol (standard deviation of the  $\text{NO}_2$  anomaly divided by the mean baseline levels of  $\text{NO}_2$  in each latitude bin) was  $< 14\%$  for both OSIRIS and MIPAS.

Figure 4 shows the correlation between  $\text{NO}_2$  VCD percent differences and AOD for all times/latitudes. Note that data between  
5  $60^\circ\text{S}$  and  $80^\circ\text{S}$  are excluded from the correlation coefficients due to large variability in the AOD, perhaps due to polar stratospheric clouds. For OSIRIS, there appears to be a negative linear relationship, with  $R = -0.68$ . For larger AODs  $> 4 \times 10^{-3}$ , OSIRIS VCDs are  $\sim 20\text{-}60\%$  lower than under baseline conditions. For MIPAS, the relationship between  $\text{NO}_2$  percent difference and AOD is weaker, with  $R = -0.37$ . When only data from  $40^\circ\text{S}$  to  $80^\circ\text{N}$  are considered, the anticorrelation is somewhat stronger, with  $R = -0.50$ . Compared with OSIRIS, there are fewer monthly average MIPAS measurements available  
10 when AODs are high, which likely contributes to the weaker correlation. For AODs  $> 4 \times 10^{-3}$ , 18 out of 19 latitude-binned MIPAS VCDs have negative percent differences, typically in the range of  $\sim 5\text{-}25\%$ .

The effect of volcanic aerosol on  $\text{NO}_2$  is smaller for MIPAS than for OSIRIS. From the model simulations in Figure 2 it appears that the difference in local time of the measurements, 10:00 vs. 06:30, can explain only a small part of this difference. Likely a larger contributor to the smaller MIPAS  $\text{NO}_2$  anomalies is a damping effect as many of the VCDs had DOFS  $< 1$ ,  
15 with smaller DOFS for larger OSIRIS partial column AODs. For OSIRIS partial column AODs  $> 5 \times 10^{-3}$ , the average MIPAS DOFS was  $\sim 0.6$ . The sub-optimal DOFS is accompanied by coarse altitude resolution which smooths  $\text{NO}_2$  from higher altitudes where aerosol levels are not enhanced. In other words, the coarse altitude resolution leads to a smaller amplitude in the local  $\text{NO}_2$  variation in the MIPAS data. Also, correlation due to an  $\text{NO}_2$  retrieval dependency on aerosol is expected to be small for OSIRIS because of the differential nature of the measurement and the spectral proximity of the selected strongly and  
20 weakly absorbing wavelengths (Bourassa et al., 2011).

The relationship between the MIPAS  $\text{N}_2\text{O}_5$  anomaly and OSIRIS aerosol is also shown in Figure 3 and Figure 4. Strong anticorrelation between the  $\text{N}_2\text{O}_5$  anomaly and AOD is observed, with  $R = -0.86$  for  $50^\circ\text{S}$  to  $80^\circ\text{N}$  and  $R = -0.90$  for  $40^\circ\text{S}$  to  $80^\circ\text{N}$ . The percentage decrease in  $\text{N}_2\text{O}_5$  cannot be inferred due to the known low bias in the MIPAS data at these altitudes. Despite this low bias, the DOFS of  $\sim 1.8$  suggest that real variability in  $\text{N}_2\text{O}_5$  is observed.

25 MIPAS  $\text{HNO}_3$  VCDs were also considered in this analysis (not shown here) using the same methodology as for  $\text{NO}_2$  and  $\text{N}_2\text{O}_5$ , but no relationship with partial column AOD was apparent in the timeseries, with  $|R| < 0.2$  for most latitudes and altitude ranges considered. This is consistent with results from the photochemical model which suggest that  $\text{HNO}_3$  should increase by less than 10% relative to baseline levels for all latitudes and partial column AODs observed in this study. Such small relative increases in  $\text{HNO}_3$  would be difficult to observe over background variability.



Scatter plots for OSIRIS AOD versus NO<sub>2</sub> VCD percent difference, at latitudes where at least one AOD > 3x10<sup>-3</sup> was recorded, are shown in Figure 5. At all latitudes, higher AODs are associated with lower levels of NO<sub>2</sub>, with R ranging from -0.40 to -0.85 at the various latitudes. For smaller AODs (< ~3x10<sup>-3</sup>), this relationship appears to be somewhat linear. For larger AODs, however, this relationship displays greater curvature with additional aerosol having an increasingly smaller impact, which is consistent with the saturation at higher aerosol levels (e.g., Fahey et al., 1993). The larger AODs are all measured following volcanic eruptions (Table 2). The modelled NO<sub>2</sub> percent differences, interpolated to the OSIRIS month, latitude, and partial column AOD are also shown. The modelled data agrees well quantitatively with the OSIRIS measurements across latitudes and AOD ranges and reproduces the shape of the curve approaching saturation.

Other species are expected to be affected by increased aerosol, including BrONO<sub>2</sub>, from Eq. (2), and by extension, BrO, where BrO is also measured by OSIRIS (McLinden et al., 2010). An analysis of the OSIRIS BrO product indicated no significant impact following the eruptions. This is consistent with a model-estimated increase in BrO of only 5-10% for AOD=8x10<sup>-3</sup> (not shown here), and the reduced sensitivity of the OSIRIS BrO product below 20 km.

#### 4.2 OSIRIS NO<sub>2</sub> profiles

The OSIRIS NO<sub>2</sub> and aerosol extinction profiles were used to assess the altitude range over which levels of NO<sub>2</sub> decreased in the presence of volcanic aerosol. The MIPAS NO<sub>2</sub> profiles were not considered because of limitations in the vertical resolution in the lower stratosphere.

The timeseries of OSIRIS extinction ratio and OSIRIS and modelled NO<sub>2</sub> profiles are shown for 0° in Figure 6. Negative NO<sub>2</sub> anomalies are apparent during the periods of enhanced aerosol for altitudes between ~16-24 km, with maximum decreases in NO<sub>2</sub> typically at ~20 km in both the OSIRIS and model datasets. These altitudes coincide approximately with the largest observed extinction ratios. OSIRIS measured percent differences in NO<sub>2</sub> of up to ~50% after the 2006 Soufrière Hills volcano, up to ~40% after the 2014 Kelut volcano, up to ~35% after the 2011 Nabro volcano, and up to ~25% after the 2005 Manam volcano. In the model dataset, similar qualitative features are observed, but with somewhat smaller reductions in NO<sub>2</sub>. Modelled percent differences reach up to ~20% after the Nabro and Manam volcanoes and up to ~30% after the Soufrière Hills and Kelut volcanoes. This is consistent with the modelling comparisons of VCDs and partial column AODs (Figure 5), in which modelled NO<sub>2</sub> percent differences at 0° latitude are biased somewhat low compared with OSIRIS. Only the aerosol extinction is varied inter-annually in the model, which likely why the model displays less variability than OSIRIS during non-volcanic periods.

At 50°N, both OSIRIS and modelled negative NO<sub>2</sub> anomalies are similarly related to the times and altitudes of enhanced levels of aerosol, as shown in Figure 7. At this latitude, decreases in NO<sub>2</sub> are observed between ~10-20 km. Decreases in NO<sub>2</sub> of up to ~50% are observed after the 2009 Sarychev Peak volcano, up to ~40% after the 2011 Nabro volcano, and up to ~30%



after the 2008 Kasatochi/Okmok volcanoes. The modelled percent difference profiles are similar to the OSIRIS data, reaching ~40% for the Sarychev Peak and Nabro volcanoes and ~30% for the Kasatochi/Okmok volcanoes.

The OSIRIS-measured variability in NO<sub>2</sub> outside of the periods of volcanic aerosol (standard deviation of the NO<sub>2</sub> anomaly divided by the mean baseline levels of NO<sub>2</sub> in each latitude/altitude bin) was < 20% for most latitude/altitude bins. Therefore, the OSIRIS-measured decreases in NO<sub>2</sub> of up to ~30-50% after these volcanic eruptions are significant compared to background variability.

At both 0° (Figure 6) and 50°N (Figure 7), positive NO<sub>2</sub> anomalies are also observed, in particular before 2005. This is in part because baseline NO<sub>2</sub> is calculated using measurements taken for aerosol ratios < 1.2. Below this threshold, levels of aerosol still vary, and tend to increase after ~2005 at most latitudes (see, for example, Figure 1). This leads to positive anomalies in NO<sub>2</sub> during periods with lower levels of volcanic aerosol, as are reflected in the photochemical model results, which are based entirely on aerosol levels. There are some differences between the OSIRIS measurements and model results during periods with positive anomalies. For example, at 0° (Figure 6), positive anomalies are stronger in the OSIRIS data than in the model output, suggesting that the observed anomaly is not fully explained by aerosol levels and may be related to other sources of variability.

At each altitude and latitude, the correlation coefficient between the OSIRIS percent difference in NO<sub>2</sub> and the aerosol extinction was calculated and is shown in Figure 8. Negative correlations between NO<sub>2</sub> and aerosol are observed at most latitudes and altitudes in the lower stratosphere. Altitudes and latitudes that were affected by volcanic aerosol for at least one month in the timeseries are given by the magenta and green contour lines. For these altitudes and latitudes, the relationship between NO<sub>2</sub> and extinction tends to be stronger. In each latitude bin, the strongest correlation coefficient across altitudes is similar to the correlation coefficients for the partial VCDs and partial column AODs shown in Figure 5. In some cases, the strongest correlation coefficient within the profile is slightly lower than for the partial VCDs and partial column AODs, suggesting noise in either the NO<sub>2</sub> or aerosol extinction profiles or both. For 60°S to 90°S, some positive correlation coefficients are observed. The variability in OSIRIS aerosol extinction at these latitudes is largely unrelated to volcanic aerosol.

## 5 Conclusion

Between 2002 and 2014, seven periods with enhanced volcanic aerosol were observed by OSIRIS and, in most cases, were associated with reduced levels of NO<sub>2</sub> observed by both OSIRIS and MIPAS. For the partial column AODs between  $5\text{-}7 \times 10^{-3}$ , OSIRIS and MIPAS NO<sub>2</sub> VCDs decrease relative to baseline levels by ~20-50% and ~5-25%, respectively. For AODs >  $7 \times 10^{-3}$ , decreases in OSIRIS NO<sub>2</sub> reached ~40-60%. No MIPAS NO<sub>2</sub> measurements were available for AODs >  $7 \times 10^{-3}$ .



MIPAS observed a smaller decrease in NO<sub>2</sub> than OSIRIS, which is consistent with differences in the DOFS < 1 for the MIPAS measurements.

The relationships between the percent differences in NO<sub>2</sub> relative to baseline levels and AODs are somewhat linear for both OSIRIS and MIPAS, with R between approximately -0.4 and -0.8 depending on the altitude and latitude range. Perfect linearity is not expected because heterogeneous chemistry becomes saturated toward larger aerosol concentrations (e.g., Fahey et al., 1993) and can vary throughout the timeseries with other factors, such as temperature and available sunlight (e.g., Coffey, 1996). The variation of OSIRIS percent differences in NO<sub>2</sub> with partial column AOD was compared against photochemical model runs. They were found to be consistent both in terms of the magnitude of percent difference and the shape of the curve as it approaches saturation.

10 A strong negative relationship was observed between MIPAS N<sub>2</sub>O<sub>5</sub> and OSIRIS AOD, with R ~ -0.9, however, no relationship was observed between MIPAS HNO<sub>3</sub> and OSIRIS AOD. The photochemical model suggests that increases in HNO<sub>3</sub> would be < 10% for the observed partial column AODs, and therefore would be difficult to detect above other sources of variability.

15 The reductions in NO<sub>2</sub> observed in the present study would amount to < 20% of the total column in the tropics and < 10% of the total column toward higher latitudes, even for the largest aerosol events. This is much smaller than the column reductions of up to 50-70% observed after the Pinatubo and El Chichón volcanoes (e.g., Coffey, 1996), where the largest reductions in the total column of NO<sub>2</sub> occurred for periods with aerosol enhancements above 25 km (Koike et al., 1993), where the bulk of the NO<sub>2</sub> column resides. The results presented here are consistent with the smaller stratospheric aerosol loads and lower altitude range of the more recent volcanoes (e.g., Rieger et al., 2015).

### Acknowledgments and Data

20 Thank you to Chris Roth for providing the principal components of QBO winds. This work was supported by the Natural Sciences and Engineering Research Council (Canada) and the Canadian Space Agency. Odin is a Swedish-led satellite project funded jointly by Sweden (SNSB), Canada (CSA), France (CNES), and Finland (Tekes). OSIRIS data are available at <http://odin-osiris.usask.ca>. IMK/IAA-generated MIPAS data used in this study are available for registered users at <http://www.imk-asf.kit.edu/english/308.php>. BF was supported by the Spanish MINECO under grant ESP2014-54362-P.



## References

- Baldwin, M. P., Gray, L. J., Dunkerton, T. J., Hamilton, K., Haynes, P. H., Randel, W. J., Holton, J. R., Alexander, M. J., Hirota, I., Horinouchi, T., Jones, D. B. A., Kinnerson, J. S., Marquardt, C., Sato, K. and Takahashi, M.: The Quasi-Biennial Oscillation, *Rev. Geophys.*, 39(2), 179–230, doi:10.1029/1999RG000073, 2001.
- 5 Bourassa, A. E., Degenstein, D. A., Gattinger, R. L. and Llewellyn, E. J.: Stratospheric aerosol retrieval with optical spectrograph and infrared imaging system limb scatter measurements, *J. Geophys. Res. Atmos.*, 112, D10217, doi:10.1029/2006JD008079, 2007.
- Bourassa, A. E., Degenstein, D. A. and Llewellyn, E. J.: SASKTRAN: A spherical geometry radiative transfer code for efficient estimation of limb scattered sunlight, *J. Quant. Spectrosc. Radiat. Transf.*, 109, 52–73,  
10 doi:10.1016/j.jqsrt.2007.07.007, 2008.
- Bourassa, A. E., Degenstein, D. A., Elash, B. J. and Llewellyn, E. J.: Evolution of the stratospheric aerosol enhancement following the eruptions of Okmok and Kasatochi: Odin-OSIRIS measurements, *J. Geophys. Res. Atmos.*, 115, D00L03, doi:10.1029/2009JD013274, 2010.
- Bourassa, A. E., McLinden, C. A., Sioris, C. E., Brohede, S., Bathgate, A. F., Llewellyn, E. J. and Degenstein, D. A.: Fast NO<sub>2</sub>  
15 retrievals from Odin-OSIRIS limb scatter measurements, *Atmos. Meas. Tech.*, 4, 965–972, doi:10.5194/amt-4-965-2011, 2011.
- Bourassa, A. E., Robock, A., Randel, W. J., Deshler, T., Rieger, L. A., Lloyd, N. D., Llewellyn, E. J. and Degenstein, D. A.: Large Volcanic Aerosol Load in the Stratosphere Linked to Asian Monsoon Transport, *Science*, 337(6090), 78–81, doi:10.1126/science.1219371, 2012a.
- 20 Bourassa, A. E., Rieger, L. A., Lloyd, N. D. and Degenstein, D. A.: Odin-OSIRIS stratospheric aerosol data product and SAGE III intercomparison, *Atmos. Chem. Phys.*, 12, 605–614, doi:10.5194/acp-12-605-2012, 2012b.
- Bourassa, A. E., Degenstein, D. A., Randel, W. J., Zawodny, J. M., Kyrölä, E., McLinden, C. A., Sioris, C. E. and Roth, C. Z.: Trends in stratospheric ozone derived from merged SAGE II and Odin-OSIRIS satellite observations, *Atmos. Chem. Phys.*, 14, 6983–6994, doi:10.5194/acp-14-6983-2014, 2014.
- 25 Brohede, S., McLinden, C. A., Urban, J., Haley, C. S., Jonsson, A. I. and Murtagh, D.: Odin stratospheric proxy NO<sub>y</sub> measurements and climatology, *Atmos. Chem. Phys.*, 8, 5731–5754, doi:10.5194/acp-8-5731-2008, 2008.



- Brohede, S. M., Haley, C. S., McLinden, C. A., Sioris, C. E., Murtagh, D. P., Petelina, S. V., Llewellyn, E. J., Bazureau, A., Goutail, F., Randall, C. E., Lumpe, J. D., Taha, G., Thomasson, L. W. and Gordley, L. L.: Validation of Odin/OSIRIS stratospheric NO<sub>2</sub> profiles, *J. Geophys. Res. Atmos.*, 112(D07310), 1–22, doi:10.1029/2006JD007586, 2007.
- Coffey, M. T.: Observations of the impact of volcanic activity on stratospheric chemistry, *J. Geophys. Res.*, 101(D3), 6767–6780, doi:10.1029/95JD03763, 1996.
- Cohen, R. C. and Murphy, J. G.: Photochemistry of NO<sub>2</sub> in Earth's Stratosphere: Constraints from Observations, *Chem. Rev.*, 103, 4985–4998, doi:10.1021/cr020647x, 2003.
- Fahey, D. W., Kawa, S. R., Woddbridge, E. L., Tin, P., Wilson, J. C., Jonsson, H. H., Dyes, J. E., Baumgardners, D., Borrmans, S., Toohey, D. W., Avallone, L. M., Proffitt, M. H., Pargitan, J., Loewenstein, M., Podolske, J. R., Salawitch, R. J., Wofsy, S. C., Ko, M. K. W., Anderson, D. E., Schoeberl, M. R. and Chan, K. R.: In situ measurements constraining the role of sulphate aerosols in mid-latitude ozone depletion, *Nature*, 363, 509–514, 1993.
- Fischer, H., Birk, M., Blom, C., Carli, B., Carlotti, M., von Clarmann, T., Delbouille, L., Dudhia, A., Ehhalt, D., Endemann, M., Flaud, J. M., Gessner, R., Kleinert, A., Koopmann, R., Langen, J., López-Puertas, M., Mosner, P., Nett, H., Oelhaf, H., Perron, G., Remedios, J., Ridolfi, M., Stiller, G. and Zander, R.: MIPAS: an instrument for atmospheric and climate research, *Atmos. Chem. Phys.*, 8, 2151–2188, doi:10.5194/acp-8-2151-2008, 2008.
- Fromm, M., Kablick III, G., Nedoluha, G., Carboni, E., Grainger, R., Campbell, J. and Lewis, J.: Correcting the record of volcanic stratospheric aerosol impact: Nabro and Sarychev Peak, *J. Geophys. Res.*, 119(17), 10343–10364, doi:10.1002/2014JD021507, 2014.
- Funke, B., López-Puertas, M., von Clarmann, T., Stiller, G. P., Fischer, H., Glatthor, N., Grabowski, U., Höpfner, M., Kellmann, S., Kiefer, M., Linden, A., Mengistu Tsidu, G., Milz, M., Steck, T. and Wang, D. Y.: Retrieval of stratospheric NO<sub>x</sub> from 5.3 and 6.2 μm nonlocal thermodynamic equilibrium emissions measured by Michelson Interferometer for Passive Atmospheric Sounding (MIPAS) on Envisat, *J. Geophys. Res.*, 110, D09302, doi:10.1029/2004JD005225, 2005.
- Funke, B., Stiller, G. P. and von Clarmann, T.: Mesospheric and stratospheric NO<sub>y</sub> produced by energetic particle precipitation during 2002 – 2012, *J. Geophys. Res.*, 119, 4429–4446, doi:10.1002/2013JD021404, 2014.
- Hansen, J. E. and Travis, L. D.: Light scattering in planetary atmospheres, *Space Sci. Rev.*, 16, 527–610, doi:10.1007/BF00168069, 1974.
- Hauchecorne, A., Bertaux, J. L., Dalaudier, F., Keckhut, P., Lemennais, P., Bekki, S., Marchand, M., Lebrun, J. C., Kyřořla,



- E., Tamminen, J., Sofieva, V., Fussen, D., Vanhellefont, F., Fanton d'Andon, O., Barrot, G., Blanot, L., Fehr, T. and Saavedra de Miguel, L.: Response of tropical stratospheric O<sub>3</sub>, NO<sub>2</sub> and NO<sub>3</sub> to the equatorial Quasi-Biennial Oscillation and to temperature as seen from GOMOS/ENVISAT, *Atmos. Chem. Phys.*, 10(18), 8873–8879, doi:10.5194/acp-10-8873-2010, 2010.
- 5 Haywood, J. M., Jones, A., Clarisse, L., Bourassa, A., Barnes, J., Telford, P., Bellouin, N., Boucher, O., Agnew, P., Clerbaux, C., Coheur, P., Degenstein, D. and Braesicke, P.: Observations of the eruption of the Sarychev volcano and simulations using the HadGEM2 climate model, *J. Geophys. Res. Atmos.*, 115, D21212, doi:10.1029/2010JD014447, 2010.
- Hommel, R., Timmreck, C., Giorgetta, M. A. and Graf, H. F.: Quasi-biennial oscillation of the tropical stratospheric aerosol layer, *Atmos. Chem. Phys.*, 15, 5557–5584, doi:10.5194/acp-15-5557-2015, 2015.
- 10 Höpfner, M., Glatthor, N., Grabowski, U., Kellmann, S., Kiefer, M., Linden, A., Orphal, J., Stiller, G., von Clarmann, T., Funke, B. and Boone, C. D.: Sulfur dioxide (SO<sub>2</sub>) as observed by MIPAS/Envisat: temporal development and spatial distribution at 15–45 km altitude, *Atmos. Chem. Phys.*, 13, 10405–10423, doi:10.5194/acp-13-10405-2013, 2013.
- Höpfner, M., Boone, C. D., Funke, B., Glatthor, N., Grabowski, U., Günther, A., Kellmann, S., Kiefer, M., Linden, A., Lossow, S., Pumphrey, H. C., Read, W. G., Roiger, A., Stiller, G., Schlager, H., von Clarmann, T. and Wissmüller, K.: Sulfur dioxide (SO<sub>2</sub>) from MIPAS in the upper troposphere and lower stratosphere 2002–2012, *Atmos. Chem. Phys.*, 15, 7017–7037, doi:10.5194/acp-15-7017-2015, 2015.
- 15 Jégou, F., Berthet, G., Brogniez, C., Renard, J.-B., François, P., Haywood, J. M., Jones, A., Bourgeois, Q., Lurton, T., Auriol, F., Godin-Beekmann, S., Guimbaud, C., Krysztofiak, G., Gaubicher, B., Chartier, M., Clarisse, L., Clerbaux, C., Balois, J. Y., Verwaerde, C. and Dageron, D.: Stratospheric aerosols from the Sarychev volcano eruption in the 2009 Arctic summer, *Atmos. Chem. Phys.*, 13, 6533–6552, doi:10.5194/acp-13-6533-2013, 2013.
- 20 Johnston, P. V., McKenzie, R. L., Keys, J. G. and Matthews, W. A.: Observations of depleted stratospheric NO<sub>2</sub> following the Pinatubo volcanic eruption, *Geophys. Res. Lett.*, 19(2), 211–213, doi:10.1029/92GL00043, 1992.
- Kalnay, E., Kanamitsu, M., Kistler, R., Collins, W., Deaven, D., Gandin, L., Iredell, M., Saha, S., White, G., Woollen, J., Zhu, Y., Chelliah, M., Ebisuzaki, W., Higgins, W., Janowiak, J., Mo, K. C., Ropelewski, C., Wang, J., Leetmaa, A., Reynolds, R.,
- 25 Jenne, R. and Dennis, J.: The NCEP/NCAR 40 Year Reanalysis Project, *Bull. Am. Meteorol. Soc.*, 77, 437–471, doi:http://dx.doi.org/10.1175/1520-0477(1996)077<0437:TNYRP>2.0.CO;2, 1996.
- Koike, M., Kondo, Y., Matthews, W. A., Johnston, P. V. and Yamazaki, K.: Decrease of stratospheric NO<sub>2</sub> caused by Pinatubo



- volcanic aerosols, *Geophys. Res. Lett.*, 20(18), 1975–1978, doi:10.1029/93GL01800, 1993.
- Kravitz, B., Robock, A. and Bourassa, A.: Negligible climatic effects from the 2008 Okmok and Kasatochi volcanic eruptions, *J. Geophys. Res.*, 115, D00L05, doi:10.1029/2009JD013525, 2010.
- Llewellyn, E. J., Lloyd, N. D., Degenstein, D. A., Gattinger, R. L., Petelina, S. V., Bourassa, A. E., Wiensz, J. . T., Ivanov, E.  
5 V., McDade, I. C., Solheim, B. H., McConnell, J. C., Haley, C. S., von Savigny, C., Sioris, C. E., McLinden, C. A., Griffioen,  
E., Kaminski, J., Evans, W. F. J., Puckrin, E., Strong, K., Wehrle, V., Hum, R. H., Kendall, D. J. W., Matsushita, J., Murtagh,  
D. P., Brohede, S., Stegman, J., Witt, G., Barnes, G., Payne, W. F., Piché, L., Smith, K., Warshaw, G., Deslauniers, D.-L.,  
Marchand, P., Richardson, E. H., King, R. A., Wevers, I., McCreath, W., Kyrölä, E., Oikarinen, L., Leppelmeier, G. W.,  
Auvinen, H., Mégie, G., Hauchecorne, A., Lefèvre, F., de La Nöe, J., Ricaud, P., Frisk, U., Sjöberg, F., von Schéele, F. and  
10 Nordh, L.: The OSIRIS instrument on the Odin spacecraft, *Can. J. Phys.*, 82, 411–422, doi:10.1139/p04-005, 2004.
- McLinden, C. A., Olsen, S. C., Hannegan, B., Wild, O., Prather, M. J. and Sundet, J.: Stratospheric ozone in 3-D models: A  
simple chemistry and the cross-tropopause flux, *J. Geophys. Res.*, 105(D11), 14653–14665, doi:10.1029/2000JD900124,  
2000.
- McLinden, C. A., Haley, C. S., Lloyd, N. D., Hendrick, F., Rozanov, A., Sinnhuber, B.-M., Goutail, F., Degenstein, D. A.,  
15 Llewellyn, E. J., Sioris, C. E., Van Roozendaal, M., Pommereau, J. P., Lotz, W. and Burrows, J. P.: Odin/OSIRIS observations  
of stratospheric BrO: Retrieval methodology, climatology, and inferred Br<sub>y</sub>, *J. Geophys. Res.*, 115, D15308,  
doi:10.1029/2009JD012488, 2010.
- McLinden, C. A., Bourassa, A. E., Brohede, S., Cooper, M., Degenstein, D. A., Evans, W. J. F., Gattinger, R. L., Haley, C. S.,  
Llewellyn, E. J., Lloyd, N. D., Loewen, P., Martin, R. V., McConnell, J. C., McDade, I. C., Murtagh, D., Rieger, L., Von  
20 Savigny, C., Sheese, P. E., Sioris, C. E., Solheim, B. and Strong, K.: Osiris: A Decade of scattered light, *Bull. Am. Meteorol.  
Soc.*, 93, 1845–1863, doi:10.1175/BAMS-D-11-00135.1, 2012.
- Mengistu Tsidu, G., von Clarmann, T., Stiller, G. P., Höpfner, M., Fischer, H., Glatthor, N., Grabowski, U., Kellmann, S.,  
Kiefer, M., Linden, A., Milz, M., Steck, T. and Wang, D. Y.: Stratospheric N<sub>2</sub>O<sub>5</sub> in the austral spring 2002 as retrieved from  
limb emission spectra recorded by the Michelson Interferometer for Passive Atmospheric Sounding (MIPAS), *J. Geophys.*  
25 *Res.*, 109, D18301, doi:10.1029/2004JD004856, 2004.
- Mills, M. J., Langford, A. O., O’Leary, T. J., Arpag, K., Miller, H. L., Proffitt, M. H. and Solomon, S.: On the relationship  
between stratospheric aerosols and nitrogen dioxide, *Geophys. Res. Lett.*, 20(12), 1187–1190, doi:10.1029/93GL01124, 1993.



- 5 Murtagh, D., Frisk, U., Merino, F., Ridal, M., Jonsson, A., Stegman, J., Witt, G., Eriksson, P., Jiménez, C., Megie, G., Noë, J. D. La, Ricaud, P., Baron, P., Pardo, J. R., Hauchcorne, A., Llewellyn, E. J., Degenstein, D. A., Gattinger, R. L., Lloyd, N. D., Evans, W. F. J., McDade, I. C., Haley, C. S., Sioris, C., von Savigny, C., Solheim, B. H., McConnell, J. C., Strong, K., Richardson, E. H., Leppelmeier, G. W., Kyrölä, E., Auvinen, H. and Oikarinen, L.: An overview of the Odin atmospheric mission, *Can. J. Phys.*, 80, 309–319, doi:10.1139/p01-157, 2002.
- Naujokat, B.: An Update of the Observed Quasi-Biennial Oscillation of the Stratospheric Winds over the Tropics, *J. Atmos. Sci.*, 43(17), 1873–1877, doi:10.1175/1520-0469(1986)043<1873:AUOTOQ>2.0.CO;2, 1986.
- O'Neill, N. T., Perro, C., Saha, A., Lesins, G., Duck, T. J., Eloranta, E. W., Nott, G. J., Hoffman, A., Karumudi, M. L., Ritter, C., Bourassa, A., Abboud, I., Carn, S. A. and Savastiouk, V.: Properties of Sarychev sulphate aerosols over the Arctic, *J. Geophys. Res.*, 117, D04203, doi:10.1029/2011JD016838, 2012.
- 10 Prata, A. J., Carn, S. A., Stohl, A. and Kerkmann, J.: Long range transport and fate of a stratospheric volcanic cloud from Soufrière Hills volcano, Montserrat, *Atmos. Chem. Phys.*, 7, 5093–5103, doi:10.5194/acp-7-5093-2007, 2007.
- Randeniya, L. K., Vohralik, P. F., Plumb, I. C. and Ryan, K. R.: Heterogenous BrONO<sub>2</sub> hydrolysis: Effect on NO<sub>2</sub> columns and ozone at high latitudes in summer, *J. Geophys. Res.*, 102(D19), 23543–23557, doi:10.1029/97JD01655, 1997.
- 15 Rieger, L. A., Bourassa, A. E. and Degenstein, D. A.: Merging the OSIRIS and SAGE II stratospheric aerosol records, *J. Geophys. Res.*, 12(17), 1–15, doi:10.1002/2015JD023133, 2015.
- Rinsland, C. P., Gunson, M. R., Abrams, M. C., Lowes, L. L., Zander, R., Mahieu, E., Goldman, A., Ko, M. K. W., Rodriguez, J. M. and Sze, N. D.: Heterogeneous conversion of N<sub>2</sub>O<sub>5</sub> to HNO<sub>3</sub> in the post-Mount Pinatubo eruption stratosphere, *J. Geophys. Res. Atmos.*, 99(D4), 8213–8219, doi:10.1029/93JD03469, 1994.
- 20 Rodríguez, L. A., Watson, I. M., Edmonds, M., Ryan, G., Hards, V., Oppenheimer, C. M. M. and Bluth, G. J. S.: SO<sub>2</sub> loss rates in the plume emitted by Soufrière Hills volcano, Montserrat, *J. Volcanol. Geotherm. Res.*, 173, 135–147, doi:10.1016/j.jvolgeores.2008.01.003, 2008.
- Sioris, C. E., Boone, C. D., Bernath, P. F., Zou, J., McElroy, C. T. and McLinden, C. A.: Atmospheric Chemistry Experiment (ACE) observations of aerosol in the upper troposphere and lower stratosphere from the Kasatochi volcanic eruption, *J. Geophys. Res.*, 115, D00L14, doi:10.1029/2009JD013469, 2010.
- 25 Textor, C.: Numerical simulation of scavenging processes in explosive volcanic eruption clouds, University of Hamburg., 1999.



Thomason, L. W., Poole, L. R. and Deshler, T.: A global climatology of stratospheric aerosol surface area density deduced from Stratospheric Aerosol and Gas Experiment II measurements: 1984–1994, *J. Geophys. Res.*, 102(D7), 8967–8976, doi:10.1029/96JD02962, 1997.

5 von Clarmann, T., Höpfner, M., Kellmann, S., Linden, A., Chauhan, S., Funke, B., Grabowski, U., Glatthor, N., Kiefer, M., Schieferdecker, T., Stiller, G. P. and Versick, S.: Retrieval of temperature, H<sub>2</sub>O, O<sub>3</sub>, HNO<sub>3</sub>, CH<sub>4</sub>, N<sub>2</sub>O, ClONO<sub>2</sub> and ClO from MIPAS reduced resolution nominal mode limb emission measurements, *Atmos. Meas. Tech.*, 2, 159–175, doi:10.5194/amt-2-159-2009, 2009.

10 Wegner, T., Groß, J.-U., von Hobe, M., Stroh, F., Sumińska-Ebersoldt, O., Volk, C. M., Hösen, E., Mitev, V., Shur, G. and Müller, R.: Heterogeneous chlorine activation on stratospheric aerosols and clouds in the Arctic polar vortex, *Atmos. Chem. Phys.*, 12, 11095–11106, doi:10.5194/acp-12-11095-2012, 2012.



Table 1: Conversion factors for aerosol extinctions measured at various wavelengths.

Conversion (nm)	Angstrom coefficient	Conversion factor (ratio of extinctions)
1020 → 525	2.5	5.42
750 → 525	2.3	2.27
1020 → 750	2.8	2.39



Table 2: Summary of volcanoes observed in OSIRIS partial column AOD and associated OSIRIS NO<sub>2</sub> VCDs. References given in footnotes describe stratospheric aerosol following these eruptions.

Volcano Name <sup>a</sup>	Eruption Date	Eruption Latitude	Extent of aerosol enhancement observed by OSIRIS <sup>b</sup>	Effect on OSIRIS-observed NO <sub>2</sub> partial VCD
Manam <sup>c</sup>	27 Jan 2005	4°S	Both hemispheres, confined to the tropics	Minimal effect on observed NO <sub>2</sub>
Soufrière Hills <sup>d</sup>	30 May 2006	17°N	Both hemispheres, reaching high latitudes in spring 2007	For 50°S-0° and 40°-60°N, NO <sub>2</sub> is lower by ~10-40%
Mt Okmok <sup>e</sup> Kasatochi <sup>e</sup>	12 Jul 2008 7 Aug 2008	53°N 52°N	Combined effect of both volcanoes, reached tropics in Dec 2008-Jan 2009	For 40-80°N NO <sub>2</sub> is lower by ~20-40%
Sarychev Peak <sup>f</sup>	12 Jun 2009	48°N	Large AODs until Dec 2010, mostly confined to northern hemisphere mid-latitudes and high latitudes	For 30-80°N, NO <sub>2</sub> is lower, reaching reductions of up to ~45-55% for 40-80°N
Mt Merapi	4 Nov 2010	7°S	Both hemispheres, small signal confined to tropics in northern hemisphere and extending to higher latitudes in southern hemisphere in Jan 2011	Minimal effect on observed NO <sub>2</sub>
Nabro <sup>g</sup>	12 Jun 2011	13°N	Large AODs throughout the northern hemisphere until Jan 2012, with smaller AODs until Jun 2012	20-80°N, NO <sub>2</sub> is lower, reaching reductions of up to ~50-55% for 50-80°N
Kelut	13 Feb 2014	8°S	Both hemispheres, confined to the tropics	For 10S°-0° NO <sub>2</sub> is lower by ~20-40%

<sup>a</sup> Eruption dates and latitudes from (Höpfner et al., 2015) and reports available at <http://volcano.si.edu/>.

<sup>b</sup> OSIRIS does not measure AOD in the winter hemisphere and therefore may not capture the full extent of aerosol enhancement.

<sup>c</sup> (Bourassa et al., 2012b)

<sup>d</sup> (Prata et al., 2007)

<sup>e</sup> (Bourassa et al., 2010; Kravitz et al., 2010; Sioris et al., 2010)

<sup>f</sup> (Haywood et al., 2010; Jégou et al., 2013; O'Neill et al., 2012)

<sup>g</sup> (Bourassa et al., 2012a)

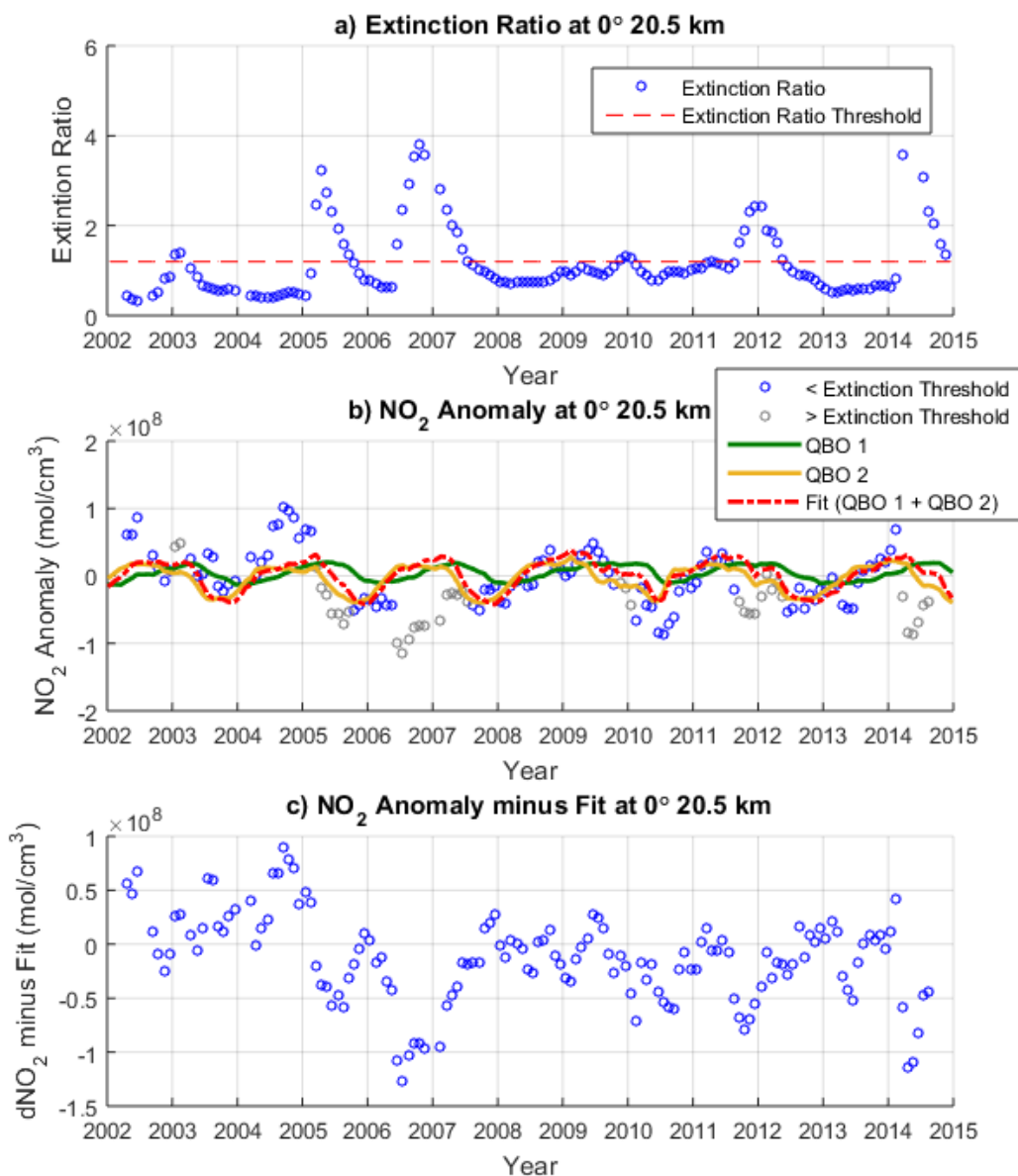


Figure 1: QBO fitting results for 0° latitude at 20.5 km. (a) Extinction ratio timeseries (blue circles) with extinction ratio threshold (red dashed line). (b) NO<sub>2</sub> anomaly timeseries for time periods with extinction ratio < extinction ratio threshold (blue circles) and time periods with extinction ratio > extinction ratio threshold (grey circles). The fits for the two QBO principal components – QBO 1 (green line) and QBO 2 (yellow line) – as well as the total fit (red dashed lined) to the NO<sub>2</sub> anomaly timeseries during time periods with extinction ratio < extinction ratio threshold are also shown. (c) NO<sub>2</sub> anomaly timeseries after subtraction of the fit.

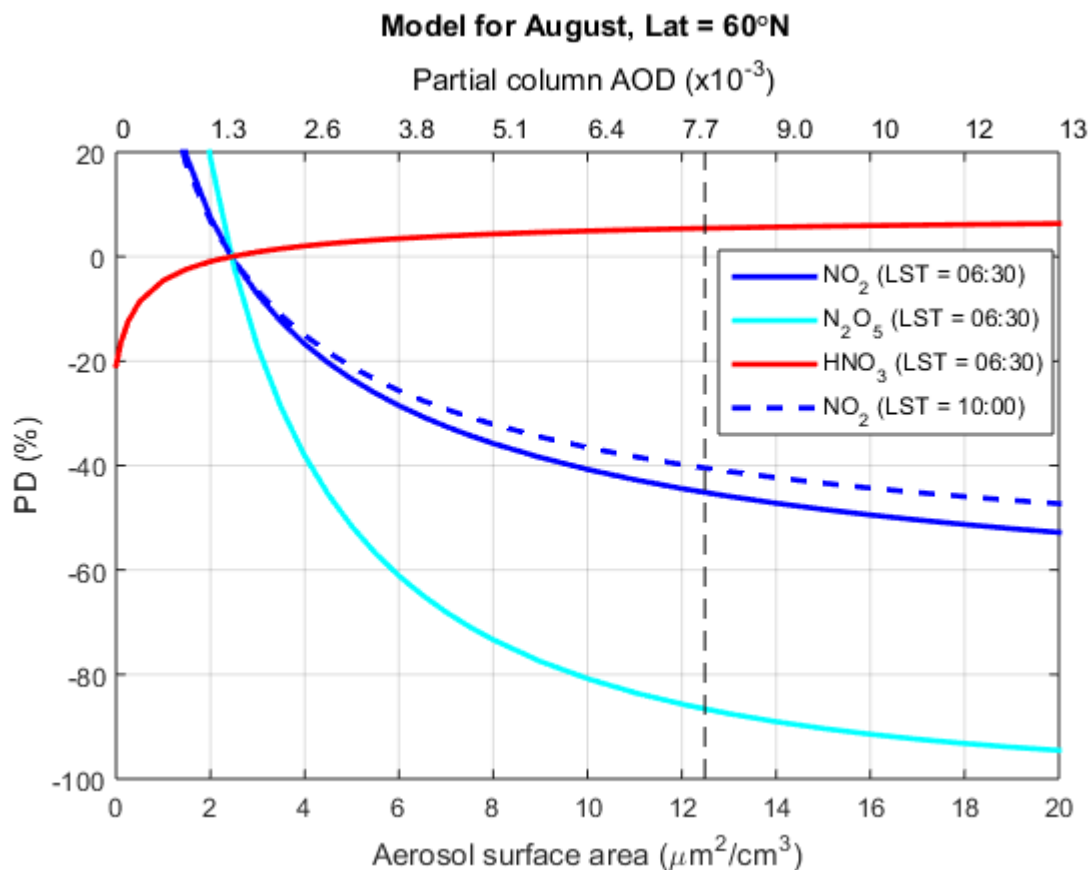


Figure 2: Modelled variations of NO<sub>2</sub>, N<sub>2</sub>O<sub>5</sub>, and HNO<sub>3</sub> with stratospheric aerosol at 60°N in August. Aerosol surface area (bottom x-axis) and partial column AOD (top x-axis) are both shown. The y-axis gives the percent difference (anomaly – baseline)/baseline for partial VCDs of NO<sub>2</sub> (blue line), N<sub>2</sub>O<sub>5</sub> (cyan line), and HNO<sub>3</sub> (red line) at the approximate OSIRIS local time (06:30 LT), and for NO<sub>2</sub> (blue dashed line) at the approximate MIPAS measurement time (10:00 LT). AODs and VCDs were calculated ~3-7 km above the tropopause. The black dashed line indicates partial column AOD =  $8 \times 10^{-3}$ , approximately the largest value in the OSIRIS measurements.

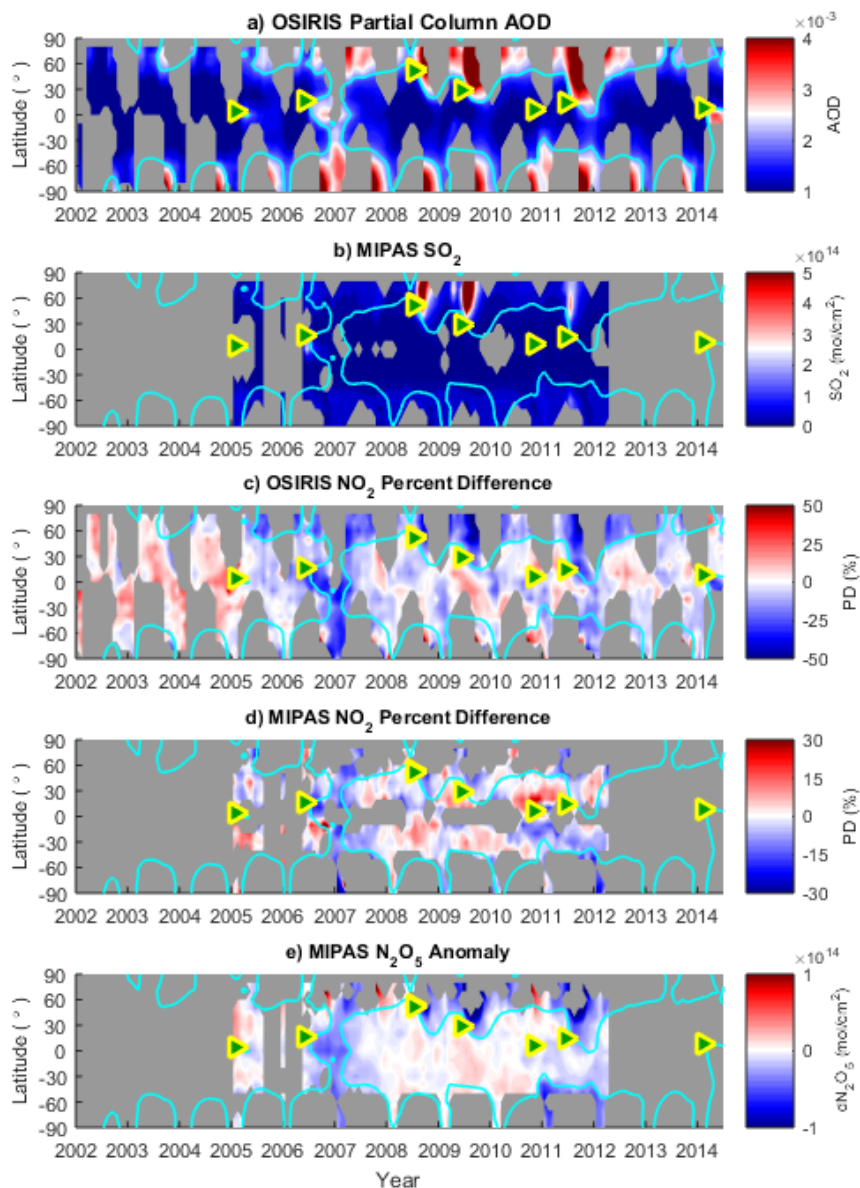


Figure 3. Contour plots of time (x-axis) versus latitude (y-axis) versus (a) OSIRIS partial column AODs, (b) MIPAS  $\text{SO}_2$  VCDs, (c) percent difference of OSIRIS  $\text{NO}_2$  VCDs, (d) percent difference of MIPAS  $\text{NO}_2$  VCDs, and (e) MIPAS  $\text{N}_2\text{O}_5$  anomaly. The partial column AODs and VCDs are calculated for 3–7 km above the thermal tropopause. Percent differences are relative to baseline levels of  $\text{NO}_2$ . Note that different colour-scale ranges are used for OSIRIS and MIPAS  $\text{NO}_2$  percent differences. The cyan contour lines show OSIRIS  $\text{AOD} = 2 \times 10^{-3}$ , extrapolated to latitudes/times where data were unavailable. The yellow/green triangles indicate the volcanic eruptions identified in Table 2.

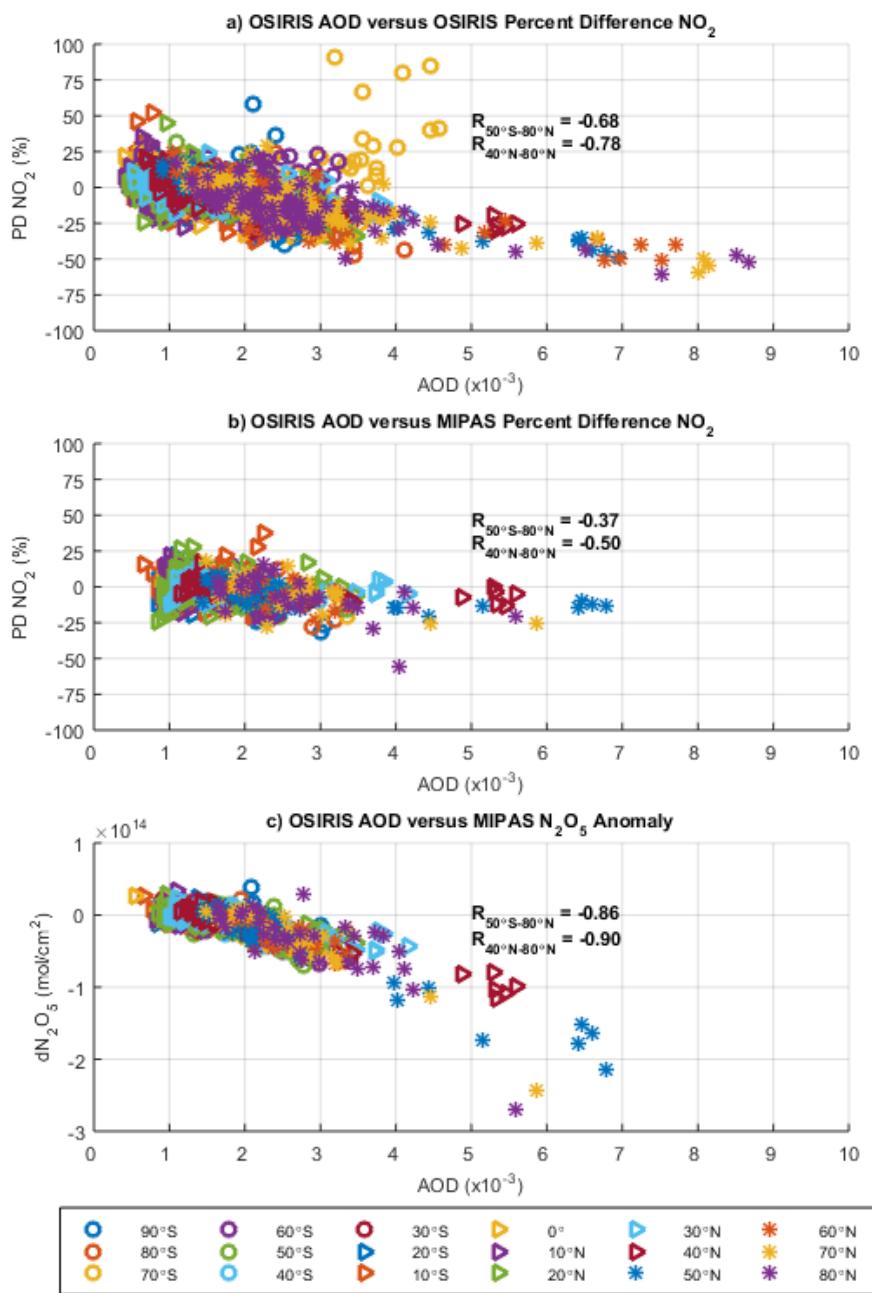


Figure 4. Scatter plots of OSIRIS AOD versus (a) OSIRIS and (b) MIPAS percent difference of NO<sub>2</sub> VCD relative to baseline levels and (c) MIPAS N<sub>2</sub>O<sub>5</sub> anomaly. The legend shows the measurement latitude. R for NO<sub>2</sub> percent difference and AOD for data collected between 50°S and 80°N, and 40°N and 80°N are given in the plot. The p-values for all calculated R are <

5 1x10<sup>-8</sup>.

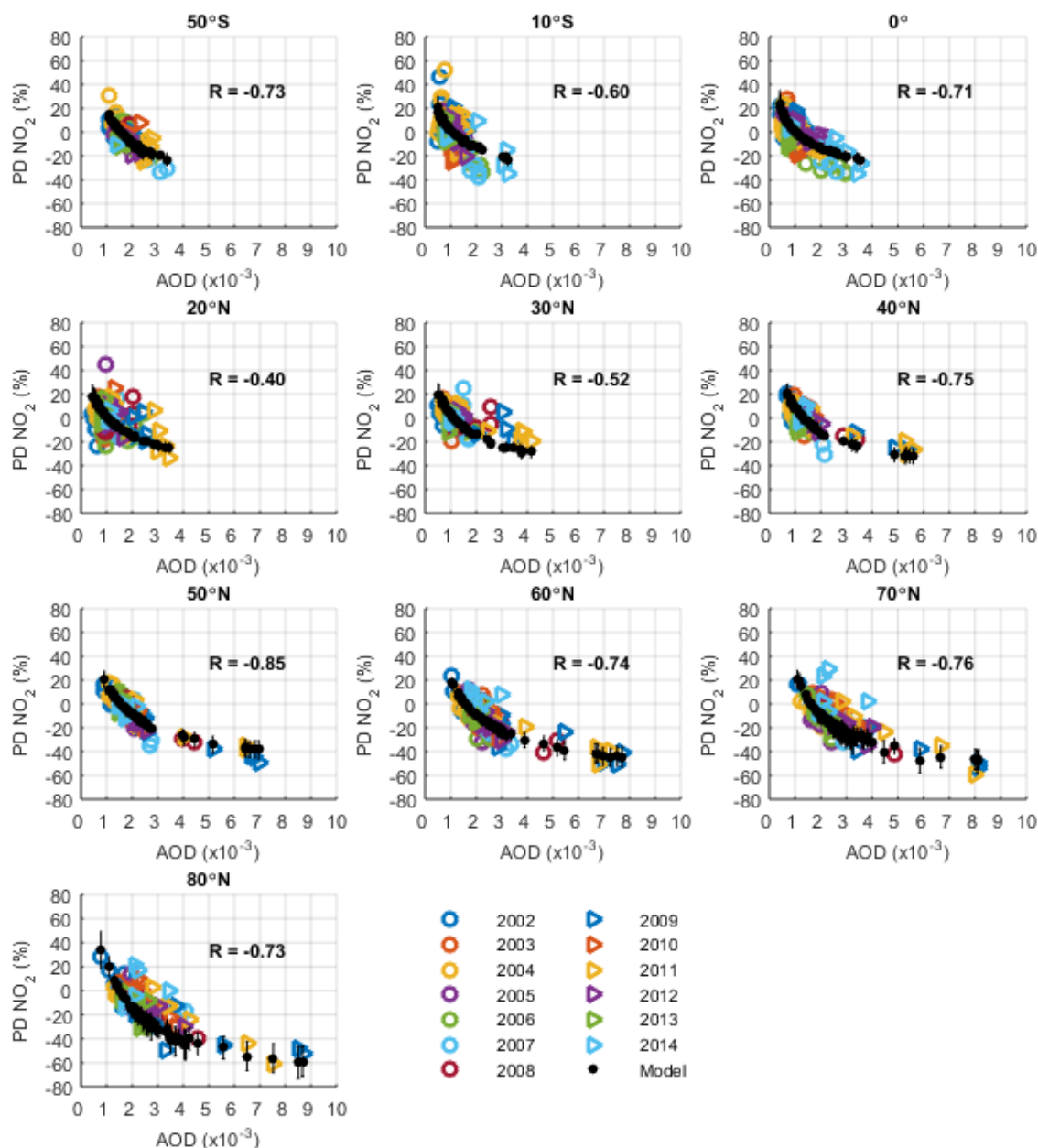


Figure 5. Scatter plots of OSIRIS AOD versus OSIRIS  $\text{NO}_2$  percent difference in VCD relative to baseline levels for various latitudes, with  $R$  given in the plot. The legend shows the measurement years. Modelled values are shown with black dots, with error bars representing uncertainties in aerosol extinction to aerosol surface area conversions, as described in Sect. 2.3.

5 The p-values for  $R$  in all panels are  $< 1 \times 10^{-5}$ .

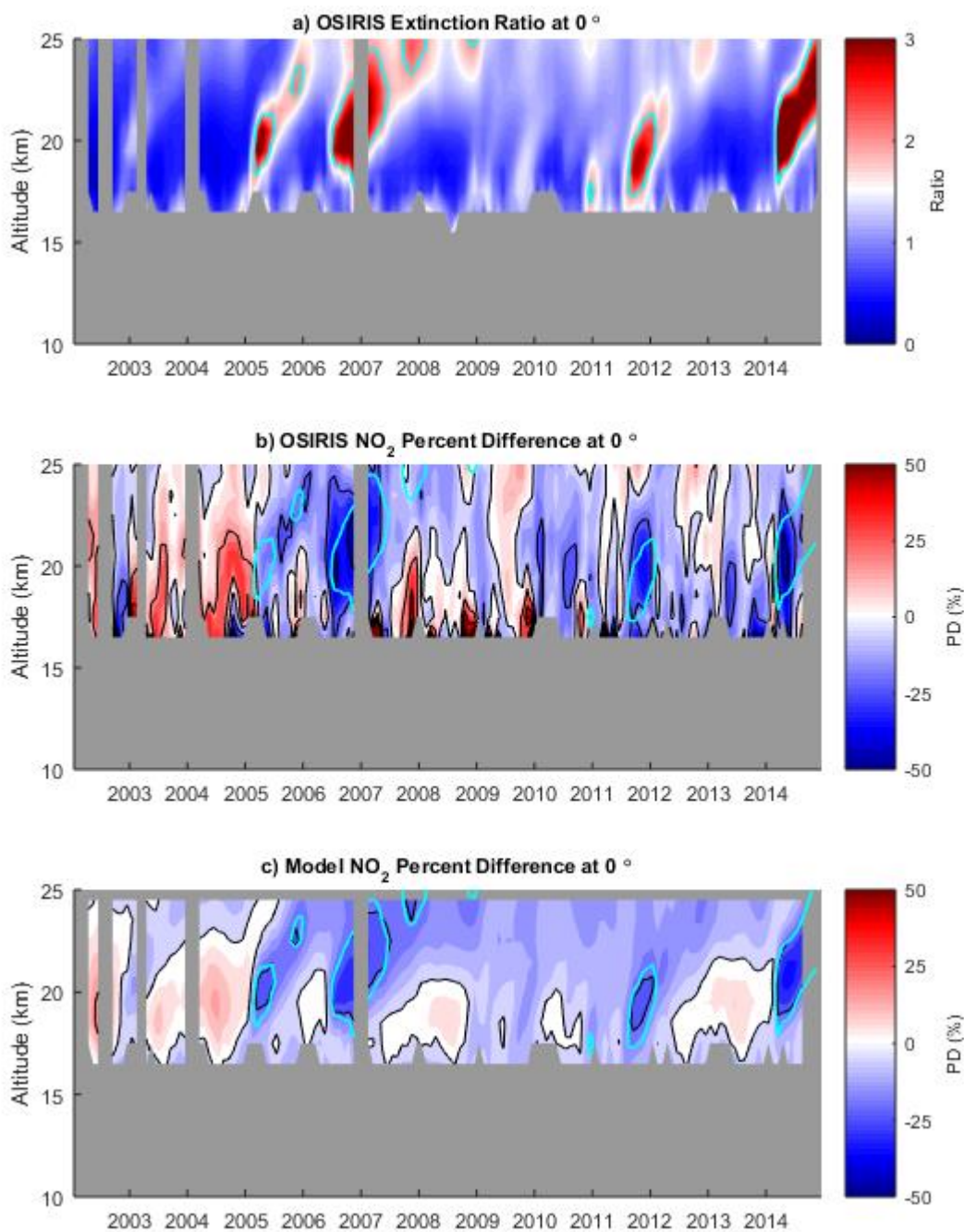


Figure 6. Profiles of aerosol extinction and  $\text{NO}_2$  percent difference at  $0^\circ$ . Timeseries of (a) OSIRIS extinction ratio, (b) OSIRIS percent difference  $\text{NO}_2$  relative to baseline levels, and (c) modelled percent difference  $\text{NO}_2$  relative to baseline levels. The thin black contour lines indicate -40%, -20%, 0%, and +20%. The cyan contours are for extinction ratios = 2.

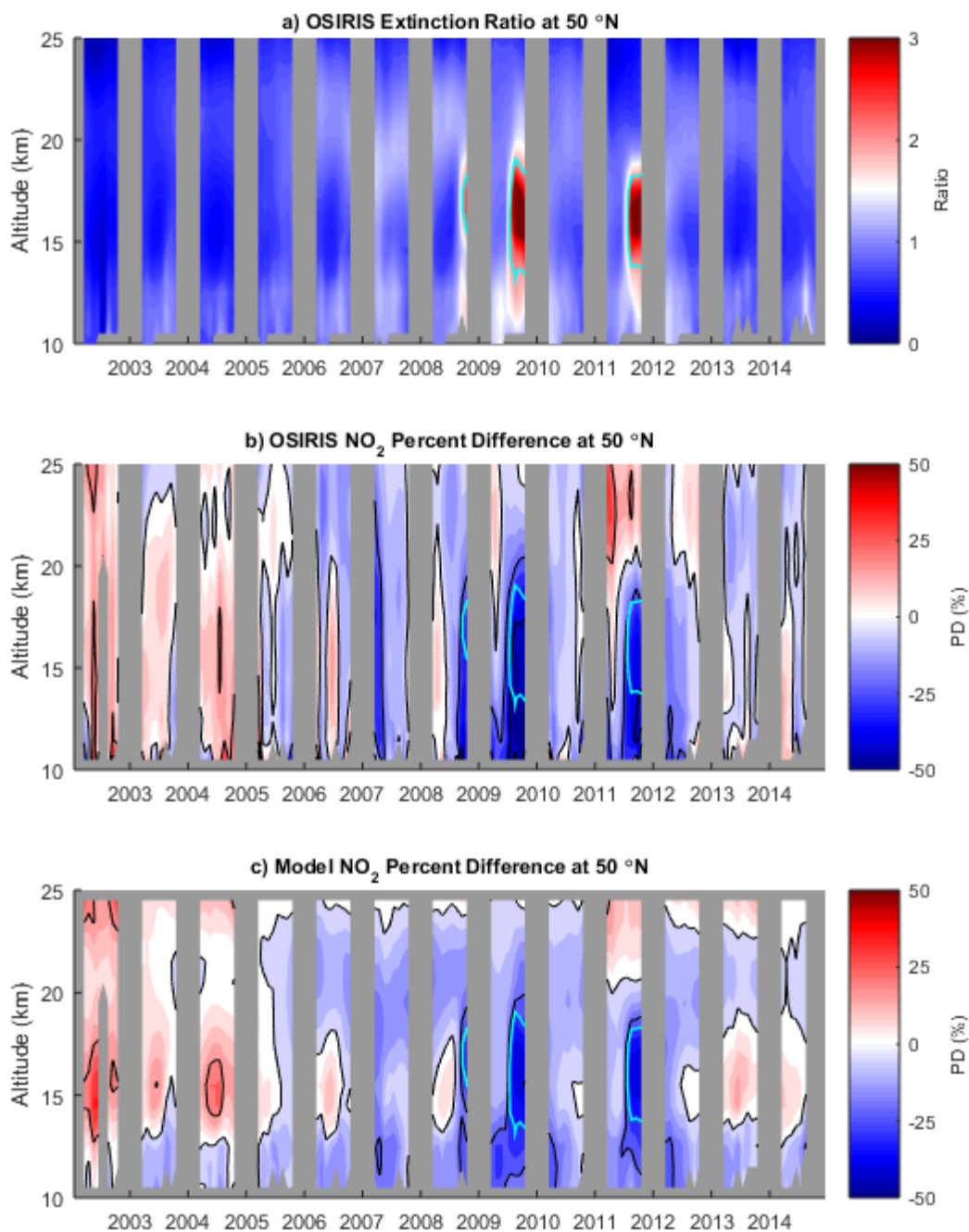


Figure 7. Profiles of aerosol extinction and NO<sub>2</sub> percent difference at 50°N. Timeseries of (a) OSIRIS extinction ratio, (b) OSIRIS percent difference NO<sub>2</sub> relative to baseline levels, and (c) modelled percent difference NO<sub>2</sub> relative to baseline levels. The thin black contour lines indicate -40%, -20%, 0%, and +20%. The cyan contours are for extinction ratios = 2.

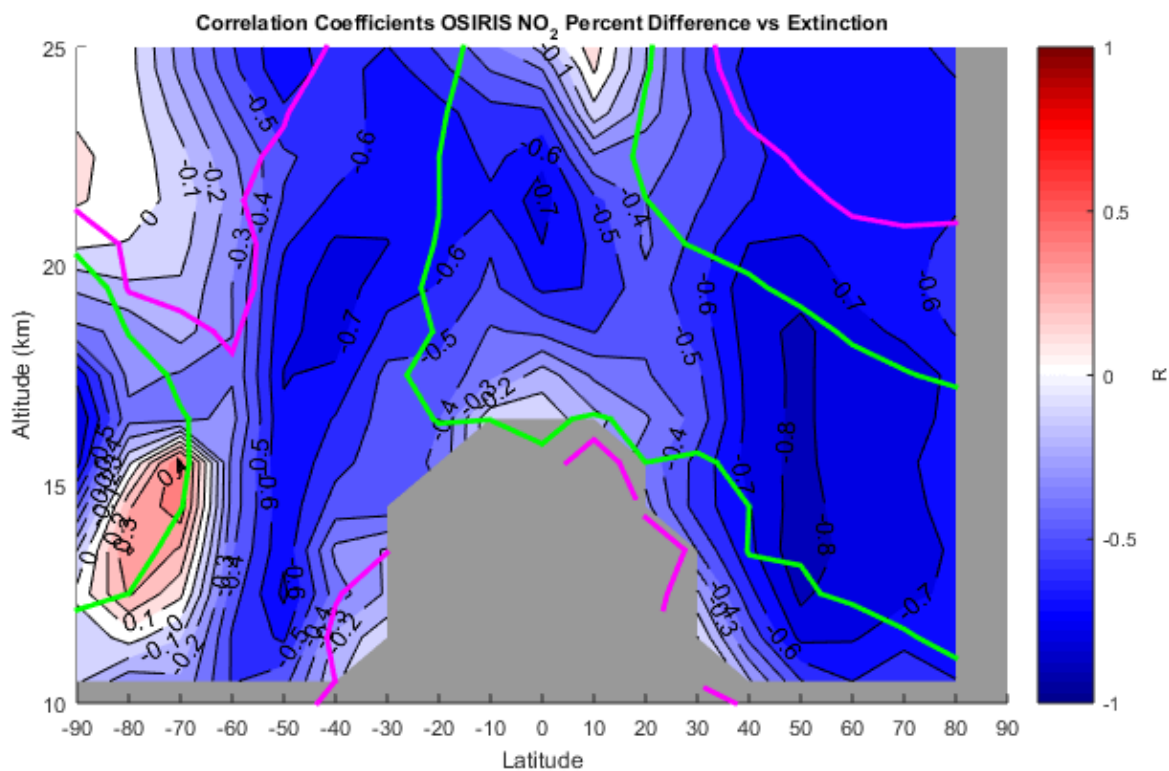


Figure 8.  $R$  for timeseries of OSIRIS percent difference in  $\text{NO}_2$  versus aerosol extinction for each latitude and altitude, the  
5 magenta and green contours are for latitudes and altitudes at which maximum extinction ratios over the timeseries was 1.2 and 2, respectively.